Seismic risk and loss estimation for the building stock in Isfahan. Part I: Exposure and Vulnerability

Mohsen Kohrangi[1], Paolo Bazzurro[2], Dimitrios Vamvatsikos[3]

[1] *RED, Risk Engineering + Development, Pavia (Formerly Research Assistant, Scuola Universitaria Superiore IUSS Pavia, Pavia, Italy); email: mohsen.kohrangi@redrisk,com; ORCID: 0000-0001-9151-0361*
[2] *Professor, IUSS, Pavia, Italy; email: paolo.bazzurro@iusspavia.it; ORICID: 0000-0001-6107-9451*
[3] *Associate Professor, School of Civil Engineering, National Technical University of Athens, Greece; email: divamva@mail.ntua.gr; ORCID: 0000-0002-4016-5040*

Abstract

This paper focuses on the exposure and fragility/vulnerability of the residential, mixed residential/commercial, and public building stock of the city of Isfahan, in Central Iran, and constitutes the first part of a seismic risk assessment study for that city. To determine the assets at risk, we first summarize the details of the building stock and population from the available georeferenced 2011 Census data. From this dataset and from a local survey of the city, we categorize the building taxonomy in 27 construction classes characterized by age, height, and material/lateral-load-resisting system. A building exposure model is then assembled by first dividing Isfahan in city blocks and then by assigning the appropriate statistical properties to the buildings, such as construction class, built area, and replacement cost. The population of each city block is also estimated and accounted for. To assess the fragility and vulnerability to earthquake ground motion, for each building class we performed nonlinear dynamic analysis of multiple equivalent single-degree-of-freedom systems. This process generated a set of class- and region-specific fragility and vulnerability functions that considered both record-to-record and building-to-building response variability. In the companion paper we used the exposure model and the fragility and vulnerability curves generated for all these asset classes to probabilistically assess the seismic risk of Isfahan.

Key words: Urban Risk Assessment, Earthquake, Isfahan, Iran

1. Introduction

Iran is located in a seismically active region with a long history of devastating earthquakes. Major recent damaging earthquakes in Iran include M7.3 Kermanshah 2017 with 630 deaths, M6.6 Bam 2003 with 26,271–43,200 deaths, M7.4 Manjil-Rudbar 1990 with 35,000–50,000 deaths, and M7.2 Buin-Zahra 1962 with 12,225 deaths, among others. These seismic events and the large number of fatalities evidently indicate that Iran is one of the most active and vulnerable zones in terms of seismic hazard and risk. The greater Isfahan (32°38′N 51°39′E) is a historical and touristic city in the center of Iran. It has a population of about 1.6 million according to the 2016 Census, the third most populous metropolitan area in Iran after Tehran and Mashhad. According to the seismic zonation of the Iranian seismic design code (ICSRDB 2014), Isfahan is located in a zone of moderate seismic hazard with reference peak ground acceleration, *PGA*, on rock equal to 0.25g for a 475 year return period. Even though the estimated seismicity of Isfahan is lower than that of other seismically active large cities in Iran (such as Tehran, Tabriz and Mashhad), the large number of vulnerable buildings, the large compact population and the importance of the post-disaster functionality of the city (i.e., resilience) for the economy of the country, call for a thorough pre-disaster seismic risk and loss estimation study.

Such studies can play a fundamental role in the sustainable development of the urban area, providing local authorities and other national or local decision makers with valuable information for the identification of appropriate risk mitigation actions. These actions include, for instance, post-disaster emergency planning, devising pre-earthquake building retrofitting campaigns, creating insurance pools, and strategic urban planning,

amongst others (Silva et al. 2015). Despite the importance of seismic risk assessment studies, to date, few have been conducted for Iran, and, to the best of our knowledge, none specifically for Isfahan. The present paper and its companion aim to partially fill this gap, by (i) establishing a state-of-the-art framework for urban seismic risk assessment from hazard analysis to exposure modeling, fragility and vulnerability assessment and finally damage and loss estimations, (ii) determining a comprehensive taxonomy for Iran that can be extended to other Middle-East countries, (iii) providing a flexible fragility and vulnerability definition process based on the yield displacement, and (iv) introducing comprehensive site-specificity in ground motion selection and fragility generation.

2. Overview of Our Seismic Risk Assessment Approach

Large earthquakes affect simultaneously many structures and associated infrastructure, causing chaos and loss to urban cities, including loss of life, direct financial loss to building properties and utility systems, and indirect loss due to the effects across regional and national economies. The significant potential for human and economic losses arising from earthquakes impacting urban infrastructure has been demonstrated by many past events, such as L'Aquila (2009), Christchurch (2011) and Tohoku (2011), to mention only some recent ones. Accurate assessment of the impact of earthquakes and implementation of risk mitigation measures require decision-support tools for quantitative seismic loss estimation. To be credible, given the random nature of the earthquake phenomenon, seismic risk estimates must be probabilistically-based. Namely, they need to take into account the uncertainty in earthquake occurrence, ground motion intensity, and nonlinear structural behavior for any given level of shaking. Hence, we will not be discussing deterministic methods here.

Every probabilistic seismic risk assessment study, in general, involves the generation and integration of three components, namely (i) a seismic hazard model for the region of interest, (ii) an exposure model that describes the "asset" (e.g., a structure) or, for urban or regional studies, the spatial distribution of assets exposed to seismic hazard (e.g., buildings and people in this study), and (iii) vulnerability functions that provide the loss distribution as a function of ground motion intensity measure (IM) for all assets at risk.

Many risk assessment tools have been developed along these general guidelines, for a large spectrum of applications. All such tools, however, are far from being identical; they vary with the objective of the study. Are the stakeholders interested in estimating safety and potential losses for a single structure or for a portfolio of buildings spatially distributed over a large area? Is the vulnerability/fragility assessment site-specific or is it generic and applicable to a region or a country? Is the assessment to be performed for a single earthquake scenario, required for urban emergency planning, or for multiple scenarios, when, for instance, annual loss values are needed, as is the case for the insurance industry? Finally, what are the risk metrics, fractiles or probability distributions important for the specific application? Clear specifications that help framing the objectives of the seismic risk study at hand are needed to select the most suitable tool and methodology to use.

For example, for a high level of accuracy in the loss estimates of a single site- and structure-specific seismic assessment, a rigorous component-based seismic loss estimation via the FEMA-P58 (2012) method could be adopted (Kohrangi et al. 2016; Mitrani-Reiser 2007; Porter et al. 2001). This method, however, requires detailed information about the site hazard, the damageability and repair cost of the structural and non-structural components and contents of the building. When dealing with a portfolio of tens of thousands of buildings, there is little or no information available to perform building-specific loss assessment; even if there was, the computational burden would not allow such detailed calculations for each and every one of the buildings considered. As such, other methodologies and frameworks are utilized for seismic loss estimation of a portfolio of buildings; they usually stand on representing the overall structural seismic behavior via class-specific fragility and vulnerability functions. Furthermore, based on available census data (or other administrative information) or field surveys, an exposure model is developed in which buildings originally located in a wide area (such as a postal/ZIP code, a county, or a CRESTA—Catastrophe Risk Evaluation and Standardizing Target Accumulations—zone) are lumped at a single site as a single "macro-structure" (Bazzurro and Park 2007).

To name one of the early tools for portfolio loss assessment, the public domain HAZUS-Earthquake (FEMA-443 2003) project provided a computer application for estimating the expected seismic losses to a portfolio of structures and infrastructure due to earthquake scenarios. The HAZUS framework is specifically useful to pre- and post-disaster activity managements but it does not provide the probability distribution of the aggregated losses required, for example, by the insurance/re-insurance industry. In the last decade, many studies were dedicated to developing and enhancing the accuracy of portfolio loss estimation accounting for different aspects of the problem dealing with uncertainty treatment, spatially correlated ground motions, stochastic modeling, geographical aggregation of assets in a portfolio and generation of fragility and vulnerability functions (Aslani et al. 2012; Bazzurro and Luco 2005; Bazzurro and Park 2007; Goda and Yoshikawa 2012; Silva 2017; Silva et al. 2015; Villar-Vega et al. 2017; Weatherill et al. 2015). Most of these advancements took place in the private sector

where catastrophe risk modelers responsible for estimating earthquake risk have generated new sophisticated tools and techniques in the field of catastrophe risk modeling and urban/regional seismic risk assessment.

We take advantage of the techniques adopted in the aforementioned state-of-the-art tools for the seismic loss estimation of Isfahan. The present article is focused on the development of the exposure database and on the description of the analytical method used for generating the fragility and vulnerability curves for classes of residential, mixed residential/commercial and public buildings. The companion paper (Kohrangi et al. 2020) instead presents the hazard and risk assessment analyses and the results of the study, namely the human and monetary loss estimates. For this purpose we developed a general building taxonomy that comprises 27 different building typologies (or construction classes) based on information extracted from both the national 2011 Census and from a local building survey of the city. We then created an exposure database using the information obtained from the population and the building 2011 Census at the urban block level, and from the spatial distribution of the building heights and built-area provided by the municipality of Isfahan. The replacement cost of buildings necessary for loss assessment is estimated from the construction cost data provided by the Iranian "National Construction Engineering Organization"[1]. Regarding the development of the vulnerability of structures, given the lack of usable damage and loss data from the region, we followed the analytical route. We developed a set of site-hazard-consistent, class-specific fragility and vulnerability functions using response history analysis of equivalent Single Degree of Freedom (SDOF) systems accounting for both record-to-record and building-to-building response variability. As input we utilized a set of ground motion records that were selected to be consistent with the hazard computed utilizing the Earthquake Model of Middle East (EMME) (Şeşetyan et al. 2018).

3. Building taxonomy and exposure model

Isfahan consists of 15 municipal districts that are distributed in a land area of about 551 km^2. According to 2011 Census data, there are more than 15,600 city blocks in Isfahan with about 485,000 individual buildings. Figure 1a shows the locations of each district on the map and Figure 1b displays the borders of the blocks as well as the number of buildings in each block. Note that the term block herein refers to a city block, i.e., a continuous piece of land outlined (but not divided) by streets or alleys; this has been the basis for data collection in the 2011 Census data.

Developing an exposure model requires information about the spatial distribution, value and characteristics related to the vulnerability of the exposed "assets" (i.e., buildings and people herein) to seismic hazard. The more precise the data, the more reliable the risk assessment outputs will be. To develop the taxonomy of buildings in the study area, as mentioned earlier, structures are grouped into categories of like buildings with similar vulnerability to earthquake ground shaking. This grouping is typically done according to the three main characteristics that govern the seismic behavior of a building structure: construction material/lateral load resisting system, year of construction (which is a proxy for the Code version used for building design, if any) and height.

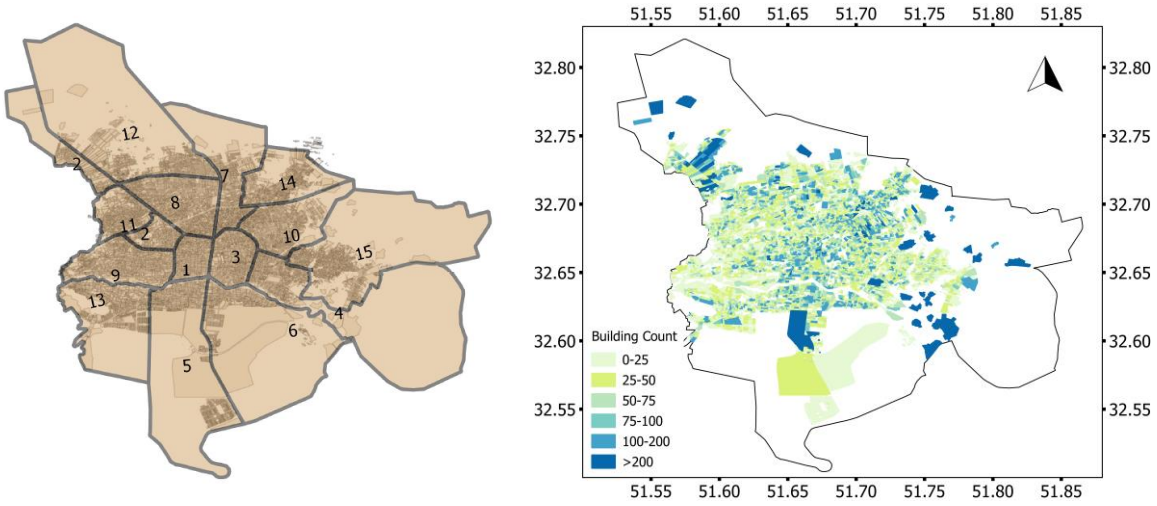

(a) (b)

Figure 1. Map of Isfahan illustrating: (a) the spatial location of the 15 districts; and, (b) building count per block.

[1] http://www.irceo.net/

Herein, to develop the exposure database we used the 2011 building and population Census data for Isfahan at the city block level together with the data at the parcel (i.e., land lot) level in terms of building height and area. The height and area values were aggregated and put into a single database. The building height was used for definition of building classes and assignment of vulnerability curves to each class while the area is used for building replacement cost. The 2011 Census also provides information about the building construction material and year as well as the number of occupants in each city block. The available information on construction material is limited to the following characterizations: "Concrete" (RC), "Steel", "Masonry" (i.e., unreinforced masonry, URM), "Adobe" and "Others". "Others" describes the buildings for which either no information is reported or the material is labeled as unknown. Herein, the "Others" category, which makes only about 0.12% of all buildings, is aggregated with the "Masonry" material type. Note that detailed information about the sub-categories of the masonry buildings (e.g., brick and wood, cement blocks, brick and steel) is also available in the Census but, for simplicity, we aggregated all these building mixed material types into the Masonry class.

The seismic design level of a structure is assumed to be consistent with the design provisions in the version of the Iranian Standard 2800 in force during the year of construction. There have been four generations of the Standard, the first covering the years of 1987–1998, and three additional from 1999 to present times, with updates every 5 to 6 years, approximately. In the latest seismic zonation map of the country (Figure 2a) Isfahan is located in an area classified as a moderate seismic zone. Figure 2b shows the design spectrum proposed by the Standard 2800 for a rock site in Isfahan and its evolution with time. There is a major difference between the first and the following three editions of the Standard, both in the amplitudes of the spectrum, generally increasing with time with the exception of the current version, and in the adoption of capacity design rules. These considerations prompted us to distinguish three major eras, namely "No-Code" (<1987 before the first edition of the code), "Mid-Code" (1987–1998, when the first edition of the code was in force) and "High-Code" (1999–now, the period of the more recent three variants of the code), respectively. Note that the changes on the seismic design level of the three "High-Code" versions of the Standard (herein considered to be otherwise equivalent), with respect to the previous version of the code are mainly confined to the moderate/long period part of the spectrum, where the latest (2012) edition of the Standard has reduced the design spectral acceleration. This change is arguably of little importance for the vast majority of the building stock with periods lower than 0.7s. Note that some limited inaccuracies in assigning each building to the corresponding pertinent version of the code may have crept in because the Census lumps the construction year of each building into eleven age brackets, some of which unfortunately straddle the years when the code changed. Thus, the "No-Code" (NC), "Mid-Code" (MC) and "High-Code" (HC) were assigned to buildings with construction year in the intervals of "<1985", "1986–1995" and ">1996", respectively. The mismatch is limited to a year or two and, therefore, it affects minimally the accuracy of the assumed earthquake design level.

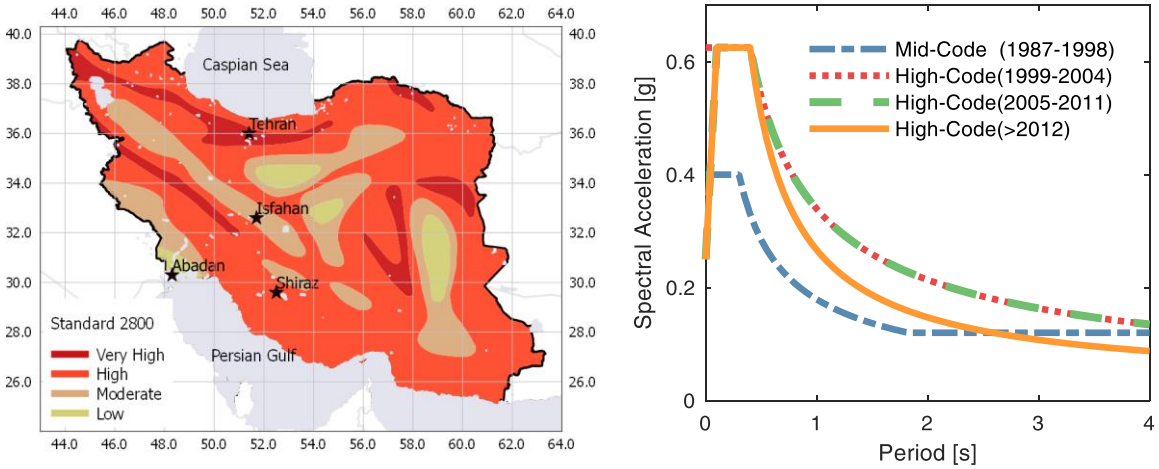

(a) (b)

Figure 2. (a) National seismic zonation map adapted from Standard 2800, version 4 (>2012) that shows the reference *PGA* on rock with values of 0.35, 0.30, 0.25, 0.20g corresponding to *"Very High"*, *"High"*, *"Moderate"* and *"Low"* seismic zones; (b) evolution of the seismic design spectrum for Isfahan for a hypothetic site located on rock.

According to the adopted NC/MC/HC classification, the buildings in the NC category are modeled to have a low seismic resistance because there were no seismic guidelines in force when they were constructed. The MC buildings are presumed to have limited seismic resistance and a moderately ductile behavior. Finally, the HC buildings are assumed to possess high strength with high levels of reserve ductility. These desirable qualities are

due to the capacity design provisions included in the latest code and to the associated advances in the building seismic design and construction practices. Even though the height and built area of buildings were also available at the parcel level (i.e. for individual buildings) since the material and construction year data were available only at the block level, we aggregated the parcel data to the block level. Finally, the height in the building classification was modeled in brackets, namely "Low-rise" (LR, i.e. 1–2 stories), "Mid-rise" (MR, i.e. 3–6 stories) and "High-rise" (HR, i.e. 7–20 stories, with 98% of the sample lying within 7–12 and only one building having 20). There is recent evidence, however, that aggregating 1-story and 2-story buildings into a single category may introduce some, albeit limited, bias in risk estimates due to the lower vulnerability of the one story buildings (Miranda and Heresi 2018). Although not undertaken herein, further splitting the LR class in one story and two story buildings is recommended in later studies.

Figure 3 shows the distribution of Material, Code (or age) and Height of the buildings in Isfahan. RC and Masonry buildings comprise about 38% of the stock each (or 75% in total), while 18% and 7% are Steel and Adobe buildings, respectively. About 31% of the buildings are expected to have limited seismic resistance (i.e., those constructed in the NC interval) and about 20% and 49% are assumed to have lateral load resistance corresponding to MC and HC categories, respectively. HC buildings tend to dominate the building stock, partly due to the construction boom of 1996 – 2011. Finally, the number of High-Rise buildings compared to the Mid-Rise and Low-Rise is significantly lower, each category respectively comprising 5%, 20% and 75% of the total number of buildings. Combining four Material types, three Height levels and three Code characteristics leads to a total of 36 building classes. Nevertheless, of the 36 total there are 15 classes that do not realistically exist in this stock (e.g., "Adobe-HC-HR" or "Masonry-HC-HR"); these are excluded resulting in a total of 21 main classes. In addition, several sub-classes that define the lateral load resisting systems for concrete and steel material are also considered. More specifically, we considered "moment-resisting frame" and "dual wall-frame" systems for RC buildings and "moment-resisting frame" and "concentrically-braced frame" systems for steel structures. These are the most common lateral load resisting systems adopted in Isfahan; other systems, such as eccentric braced frames, are only rarely used and, therefore, they are not considered herein. Based on our field survey of the city and by eliciting the opinion of several experienced engineers, we also estimated how often different load resisting systems are utilized in building construction practice. For instance, most of the Mid-Rise and all the High-Rise RC buildings in the HC interval utilize "dual wall-frame" systems, whereas "moment-resisting frames" are mostly used for LR-MC, LR-HC, MR-MC and some MR-HC RC buildings.

As a result of this classification, 27 building vulnerability classes are considered comprising the most representative buildings in Isfahan and, probably, those in most major cities in Iran. Using the 2011 Census data in each city block the number of buildings for each class is determined and spatially assigned to the geographical center of each block. In addition, the distribution of the buildings' built area with respect to their height is computed for each district and utilized to consistently assign the building area to randomly-drawn building samples when generating the exposure model. Note that, although customarily done, assigning a lumped set of buildings to the center of a block may introduce bias to the portfolio loss estimates. This operation considers all buildings in a specified block as if they were all located at its centroid creating, rather artificially, a single macro-structure for each building class in this block. For each building class, the replacement value of the macro-structure is assumed to be the sum of the replacement values of all the structures of that class in that block. Such relocation of the buildings at the centroid implies two simplifications: (a) identical ground motion generated by an earthquake for all buildings in a block, and (b) same level of damage experienced by all buildings in a given class after every earthquake. A thorough discussion of this issue is provided in Bazzurro and Park (2007). Herein, while we acknowledge this possible source of bias, we also claim that, given the rather small size of the considered city blocks (an average area of 0.0107 km^2), the actual impact of this assumption is negligible.

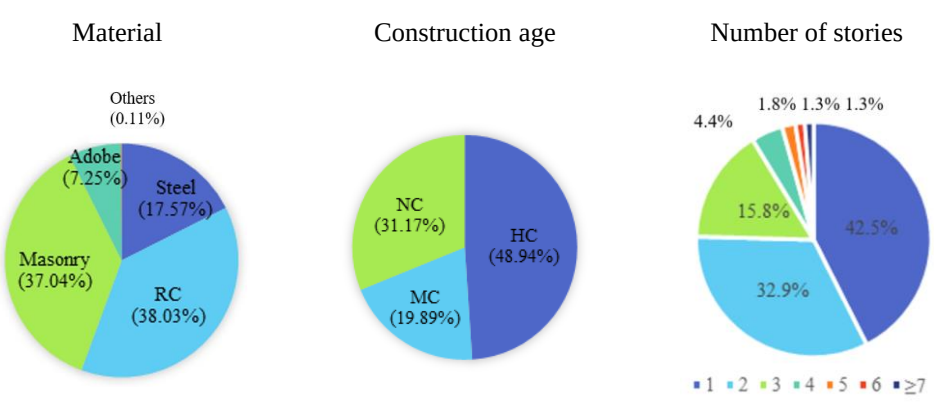

(a) (b) (c)

Figure 3. Pie charts for Isfahan's building stock based on: a) Construction material; b) Construction year (legend: NC: No-Code, MC: Mid-Code, HC: High-Code); and c) Number of stories.

The building replacement cost is established as the required monetary value to construct a building with the same characteristics of the existing one according to current costs without including costs for building code upgrade, when necessary. The National Construction Engineering Organization annually defines the acceptable construction cost per unit of covered area for the entire country as a function of the number of stories. Table 1 shows the construction cost values (in €) based on the latest issued law for 2016–2017. Employing such values assumes that, e.g., an adobe building would be replaced by an RC, reinforced-masonry or steel one, which is indeed the current reconstruction practice in Isfahan, as URM and adobe are not allowed. This obviously makes our monetary losses more representative of the actual reconstruction costs rather than the insurance payout, which would only cover the cost of the old (and cheaper) building. Still, normalized losses (e.g., vulnerability curves) provided per building class are applicable for both uses. Although these values could be materially different for different types of construction and regions in the country (or even in the city) and also could be subject to fluctuations due to international currency exchange rates, they still provide an acceptable basis to compute building replacement costs in a seismic loss assessment study. The total building cost is thus computed as the product of building area, the number of stories and the replacement cost per unit area for each assigned building in the exposure model. Finally, based on the population of each block and the total covered area, a corresponding number of residents are assigned to buildings of a given class in each block. The collection of the population per building class constitutes the human exposure subject to the seismic threat.

Table 1. Mean building construction/replacement cost per m^2 based on the latest issued law for 2017–2018. An exchange rate of 1 EUR = 50,000 IRR was assumed, matching the average rate established by the Iranian central bank for June 2018.

Number of stories	1–2	3–5	6–7	8–10	11–12	13–15	>15
Mean replacement cost (€/m^2)*	168.6	178.8	219.2	249.6	276.6	315.3	354.1

* According to the National Construction Engineering Organization these values can be 25% higher or lower. Therefore, in our exposure replacement-cost assignment process we considered a uniform distribution from 0.75 to 1.25 times the values given above.

Figure 4 shows the distribution of buildings according to the three salient characteristics of Material, Age, and Height. It is interesting to note that a large percentage of the buildings is classified as Low-rise, No-Code masonry buildings while few Mid-rise and no High-rise masonry buildings are identified. These masonry building classes are expected to be the most vulnerable and their large number increases the overall vulnerability of the city. On the other hand, 48.9% of the buildings (Figure 3) were constructed in the High-code era, rendering almost half of the city considerably less vulnerable. Based on the statistics of permits issued by the municipality in the last ten years, out of the High-code buildings, roughly two thirds are RC buildings and one third steel (Figure 4a).

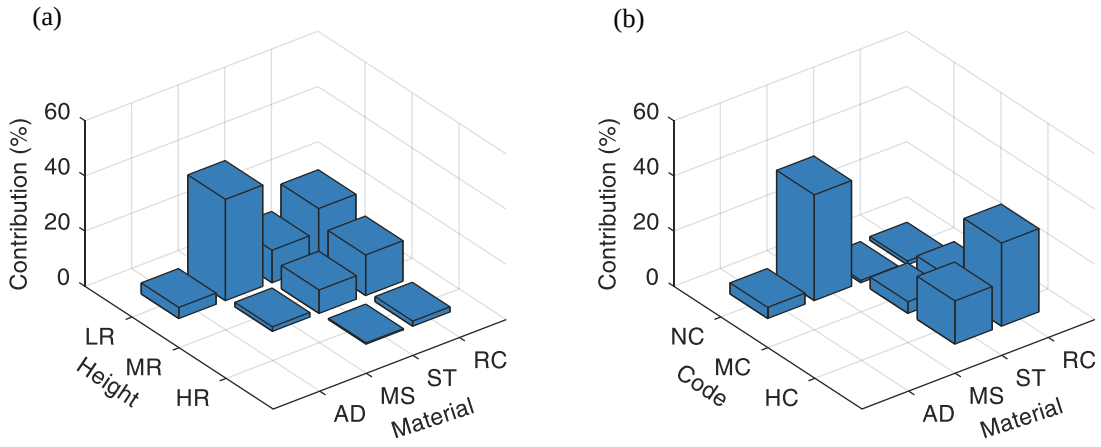

Figure 4. Distribution of buildings in the Isfahan exposure model according to type of construction, year of construction, and number of stories.

4. Fragility and Vulnerability analyses

We perform seismic damage analysis and loss calculations through the employment of fragility and vulnerability functions. A fragility function provides the probability that a building experiencing any given level of ground motion intensity (e.g., *PGA* of, say, 0.3g or 1.0g) is at the end of the shaking in a specific damage state (e.g., minor damage, moderate damage, severe damage, or collapse) or worse. A vulnerability function, a fundamental component in the process of assessing seismic risk, is defined as the probabilistic distribution of loss ratio (i.e., loss due to repair cost normalized by the replacement value of the building) conditional on any given level of ground motion intensity. Fragility functions per se do not carry any information about monetary losses. In earthquake risk assessment, they are routinely used to estimate, say, the number of unusable or collapsed buildings or of casualties after an earthquake. Alternatively, when costs are associated to each damage state by what is customarily called a consequence model (e.g., see FEMA-443 (2003)), they are utilized to develop vulnerability curves.

Building damage and repair cost data from past earthquakes can be used to empirically derive both fragility and consequence functions (e.g., Rota et al. (2008)). However, it is very uncommon for post-earthquake damage and repair cost data to be collected in such a way to allow developing empirical vulnerability functions. This gap is filled by employing analytical methods that analyze structural models of one or more structures chosen to represent the distribution of different buildings within a class.

Several studies based on empirical and analytical methods established fragility and vulnerability curves for the typical Iranian building stock (Fallah Tafti et al. 2020; Ghayamghamian and Khanzadeh 2008; Ghodrati Amiri et al. 2014; Hisada et al. 2005; Hosseini and Majd 2011; JICA 2000; Kazemi et al. 2013; Mostafaei and Kabeyasawa 2004; Ranjbaran and Hosseini 2012; Shabakhti and Biari 2013; Tavakoli and Favakoli 1993; Tobita et al. 2007). One of the earliest studies Tavakoli and Favakoli (1993), derived empirical fragility curves based on the building damage data from the M7.4 Manjil–Rudbar 1990 earthquake. The JICA project (JICA 2000) for seismic risk assessment of the greater Tehran developed several vulnerability curves for typical buildings in Tehran based on limited empirical data, a numerical method (based on capacity spectrum method), and engineering judgement. Mansouri et al. (2010) investigated four different approaches, from empirical to numerical, to derive vulnerability curves for different classes of buildings accounting for material, year (or quality) of construction and the building height for a case study seismic loss estimation for Tehran. Sadeghi et al. (2015) empirically compiled a comprehensive database of vulnerability curves to use for seismic risk assessment over the entire Iran by scrutinizing a large database of the previous studies for Iran and other countries with similar seismicity and construction practice.

In general, fragility and vulnerability curves of buildings are dependent on many factors encompassing the design and construction practice but also, in more than one way, the nature of the seismic hazard for the specific region. For instance, the buildings designed and constructed in Isfahan, being located in the moderate seismic zone according to Standard 2800, are affected both by the choice of the lateral load resisting systems and by the code-mandated lateral strength. In addition, buildings built to the same standard in different eras, have sometimes shown systematic differences due to different levels of code compliance. For example, structures constructed during the 1996-2011 boom, an era otherwise characterized as high-code, were sometimes found to have deficient construction quality as found in (Alavi et al. 2018) from studying damages in the Kermanshah earthquake. Region-specific case studies would be needed to verify the actual degree of compliance in the urban area of Isfahan, which at present are not available . Furthermore, fragility and vulnerability curves are also dependent on the site hazard, as clearly proved by Kohrangi et al. (2017) where such curves for a single identical building located at different locations with different seismicity are shown to be different. Finally, the choice of an efficient, class-specific IM to condition fragility curves is also a crucial feature for their development. An inferior choice of the IM can significantly increase the uncertainty in the final vulnerability curves and consequently in the final loss results. Herein, following this premise, we shall generate class- and site-specific fragility and vulnerability curves for the 27 building classes considered for Isfahan.

4.1 Building models

The first step in developing analytical fragility or vulnerability curves is to create appropriate building models for each class of buildings. These models may be assembled either for a few carefully selected representative “index” structure(s) (D’Ayala et al. 2014; Porter et al. 2014; Silva et al. 2015) typically designed and modelled in detail as nonlinear multi-degree-of-freedom systems (MDOFs), or for a larger set of structures (Borzi et al. 2008; Jorge and Eduardo 2007; Villar-Vega et al. 2017) but often modelled as nonlinear single-degree-of-freedom oscillators (SDOFs) to limit the computational burden.

The advantages of the simplified models are: (a) their response is not computationally intensive to compute and, (b) the within-class building-to-building response variability is accounted for. The main disadvantage, however, is that an accurate prediction of structural responses is not guaranteed, especially if higher mode effects are significant (e.g., for tall, plan asymmetric, or vertically irregular structures) and if the estimation of forces/moments/deformations along the height of a structure is of interest. In both approaches the nonlinear SDOF/MDOF models are analyzed by subjecting them to either nonlinear static pushover analysis (NSP) or nonlinear dynamic analysis (NDA). The distinction between NSP and NDA and their implementation for generating building fragility and vulnerability curves as well as discussions on the accuracy of each are provided in Silva et al. (2014b).

For a probabilistic seismic loss estimation of a large number of structures, both approaches are suitable. Here we chose NDA and use a large number of randomly generated equivalent SDOF systems that are representative of the family of buildings within each specific class. To parameterize the equivalent SDOF models, we followed the formulation of Vamvatsikos and Aschheim (2016), who employed equivalent SDOFs as a proxy for performance-based design of MDOF buildings. This approach requires 8+1 parameters, or eight scalar parameters plus a "scalable" backbone shape (i.e., a parametric vector) that is parameterized on its yield point. The eight scalars are:

i. Γ, the first-mode participation factor for the roof displacement, estimated for an eigenmode shape normalized to be 1.0 at the roof level, as typically done for pushover analysis;
ii. a_1, the first-mode mass participation factor, which is assumed to be equal to 1.0 for the case at hand, see for example Katsanos and Vamvatsikos (2017);
iii. ξ, the conventional damping ratio;
iv. C_y, the yield base shear coefficient, i.e., the yield base shear V_y normalized by the weight W, numerically equivalent to the yield spectral acceleration Sa_y in units of g: $C_y = Sa_y/\mathrm{g} = V_y/W$;
v. θ_y, the (nominal) yield story drift beyond which the response exceeds the (nominally) elastic response segment of the MDOF structure;
vi. N_{st}, the number of stories;
vii. H_{st}, the typical building storey height;
viii. a_{COD}, the coefficient of distortion, defined as the maximum interstory drift θ_{max} over the height divided by the concurrent roof drift θ_{roof}: $a_{\mathrm{COD}} \equiv \theta_{max}/\theta_{roof}$ (Moehle 1992). This ratio is herein taken to be relatively constant up to the yield point and even up to the point of maximum base shear. However, in general it tends to increase rapidly in the post-capping negative stiffness region due to localization of plastic deformations even in capacity-designed buildings (Katsanos and Vamvatsikos 2017), an effect that is herein disregarded. For a single-story structure, of course, $a_{\mathrm{COD}} = 1.0$, while for multi-story ones a_{COD} typically ranges between 1.1 and 1.4. When a softstory is present, deformation tends to localize there, leading to the higher a_{COD} values. In general, a_{COD} is a simple way of characterizing the deformation profile of the structure, while incorporating our understanding of the failure mechanism and the localization of story deformations across the height.

All other properties of the equivalent SDOF can be derived from the aforementioned data. For example, the equivalent SDOF yield displacement, δ_y, or spectral displacement at yield, Sd_y, can be computed as (Vamvatsikos and Aschheim 2016):

$$\delta_y = Sd_y = \frac{\theta_y \cdot (N_{st} \cdot H_{st})}{\Gamma \cdot a_{\mathrm{COD}}}, \tag{1}$$

while the corresponding period becomes:

$$T = 2\pi \sqrt{\frac{\delta_y}{C_y g}}. \tag{2}$$

As far as the backbone shape is concerned, the simplest possible option that could realistically represent a structure is an elastic-plastic backbone that terminates at a given ultimate global ductility, μ_u (Figure 5a). In the aforementioned formulation, a wealth of other more complex shapes that better represent realistic buildings can be employed (a) by making sure that an ultimate ductility point is always present and (b) by expressing the corresponding base shear, V, and displacement, δ, in terms of "scalable" coordinates of normalized base shear, V/V_y, and global ductility, $\mu = \delta/\delta_y$, respectively. For instance, Figure 5b shows the generic backbone curve proposed by FEMA440a (2009) expressed by the maximum inter-story drift ratio $\theta_{\max}$ versus the base shear strength of the system normalized by its yield value, F/F_y. Table 2 shows the values of the backbone capacity boundary control points (i.e., the coordinates of points B, C, D, E, F and G in Figure 5b) for four different lateral

load resisting systems corresponding to "non-ductile moment frame", "ductile moment frame", "stiff non-ductile system" and "limited-ductile moment frame", identified as spring "2a", "3a", "4a" and "7a" in FEMA-P440a, respectively. Given that Iran has followed US code practice for engineered RC and steel structures, albeit with lower compliance, it follows that similar generic macro building behaviors would hold for both countries. Thus, such parametric capacity curve shapes, herein assumed to have no cyclic degradation, are used together with the eight general building characteristics to define the actual equivalent SDOF capacity curves for Isfahan. More information is provided in the following subsections.

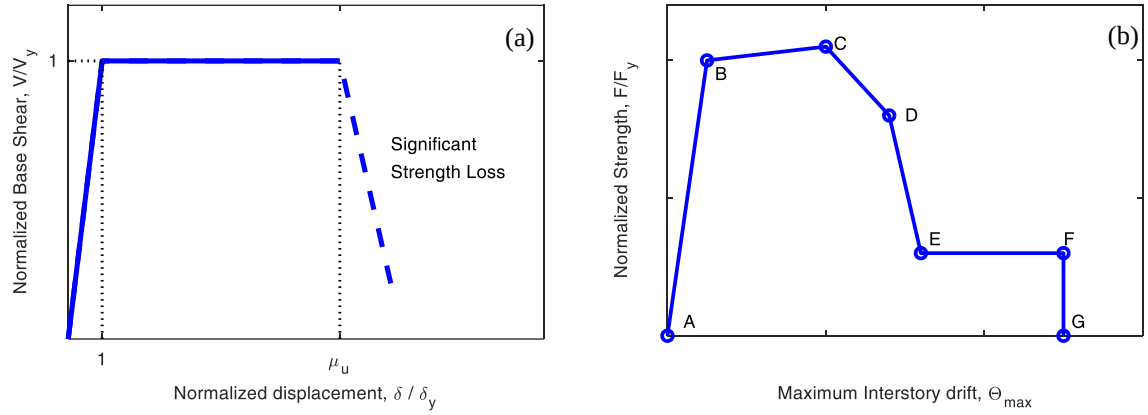

Figure 5. a) The simplest possible normalized backbone shape, an elasto-plastic model with ultimate ductility limit μ_u; b) generic backbone curve proposed by FEMA440a (2009).

Arguably the best way of estimating the values of the aforementioned 8+1 parameters would be to consider a pool (i.e., sample) of existing buildings belonging a given class in the region of interest, to perform pushover analysis for each one, and then use the results to derive the joint parameter distribution for the entire class. Herein, due to the lack of such sample data we provide our best estimates for the parameters of the capacity curves using the available literature. To do so, we define a "central" point of these 8+1 parameters for each class and assume independence among them. Then for each building class we generated 100 realizations by varying the 8+1 parameters to account for the intra-building (within-building) uncertainty in the geometrical and material properties as well as the inter-building (building-to-building) variability. Specific details on the determination of the distribution of each parameter are provided in the next sections.

Table 2. Coordinates of the backbone capacity boundary control points in terms of normalized force versus maximum inter story drift for the springs considered in this study. These values were excerpted from FEMA440a (2009) for frames and from Dolšek and Fajfar (2008) for infills. Refer to Figure 5b for their schematic illustration and Figure 6 for actual shapes and hysteretic behavior.

Structural system	**Spring**	**Quantity**	**B**	**C**	**D**	**E**	**F**	**G**
Non-ductile moment frame	"2a"	F/F_y	1.00	0.15	0.15	0.15	0.15	0.00
		θ	0.01	0.03	0.05	0.06	0.06	0.06
Ductile moment frame	"3a"	F/F_y	1.00	1.05	0.45	0.45	0.45	0.00
		θ	0.01	0.04	0.06	0.08	0.08	0.08
Stiff non-ductile system	"4a"	F/F_y	1.00	0.30	0.30	0.30	0.30	0.00
		θ	0.004	0.02	0.06	0.08	0.08	0.08
Limited ductile moment frame	"7a"	F/F_y	1.00	1.00	0.20	0.20	0.20	0.00
		θ	0.01	0.02	0.04	0.06	0.06	0.06
Infill walls	"*inf*"	F/F_y	0.67	1.00	0.00	0.00	0.00	0.00
		θ	0.002	0.005	0.01	0.03	0.04	0.06

4.1.1. URM and adobe capacity curves

Given the prevalence of low-rise URM and adobe buildings in Isfahan and the scarcity of data on their behavior, it is to be expected that the assumptions employed will play a significant role in the end results. We use elasto-plastic capacity curves for these building classes based on the recommendations of Lagomarsino and Giovinazzi (2006). The latter assumes multiple sub-classes for the URM class based on height and masonry type, such as rubble stone, simple stone, or bricks. It defines elasto-plastic SDOF systems parameterized by the yield spectral acceleration, yield spectral displacement and the ultimate displacement, which in our terminology correspond to C_y, δ_y and an ultimate ductility μ_u, respectively. The mean/median value for each of these parameters among all

of the sub-classes is used herein to define the "central value" capacity curves. The family of capacity curves for each class is obtained by multiplying the central value of these three parameters by factors uniformly distributed within [0.8, 1.2].

4.1.2. No-Code RC and steel capacity curves

The No-Code RC and steel building classes suffer both from low lateral strength and low ductility capacity. For these classes we use the "non-ductile moment frame" backbone curve, i.e., spring "2a" in FEMA-440a (2009), whose capacity curve and hysteretic behavior are shown in Figure 6a. For these No-Code buildings there is little guidance for the expected seismic capacity. Still, they can be assumed to possess low lateral seismic strength compared to the code-based designed ones. Based on engineering judgment, we assume a yield base shear coefficient C_y uniformly varying between 0.05–0.15. These assumed values are in line with those by Lagomarsino and Giovinazzi (2006), which reported C_y in the range of 0.07–0.20g for European non-designed RC moment frame buildings. The lower values assumed herein for the lower and upper bounds of the C_y range intend to account for the scarce knowledge of seismic design provisions and of appropriate construction details by Iranian practicing engineers in those early years. Also, no minimal lateral force was mandated during design in Iran. Europe adopted seismic codes much earlier (e.g., Greece had its first seismic code in 1959). We also define a coefficient of distortion (a_{COD}) by a uniform distribution in the range [1.25, 1.35].

4.1.3. Mid/High-Code RC and steel capacity curves

For each one of the code based RC and steel building classes shown in Table 3, a basic backbone force-displacement curve is adopted from FEMA440a (2009). We assume that Mid-Code RC and steel building moment frame classes are designed based on the early version of Standard 2800 and thus have considerable lateral seismic strength. Yet, they may lack in ductility capacity because of the unfamiliarity of the designers and constructors of the time with capacity design. Thus, we selected the "limited-ductility moment frame" backbone curve, i.e., spring "7a" (Figure 6d) for the RC and steel buildings in this construction era.

Table 3. Building classes, adopted values for the definitions of equivalent SDOFs backbone curves, and the resulting fragility curve parameters.

Class Description	Acronym	N_{st}	*backbone shape*	Γ[¶]	a_{COD}[¶¶]	T^*[‡]	R[♦]	Ω_o[♣]	Fragility Curves Parameters							
									Slight		Moderate		Extensive		Collapse	
									$\mu_{\ln IM}$	$\beta_{\ln IM}$	$\mu_{\ln IM}$	$\beta_{\ln IM}$	$\mu_{\ln IM}$	$\beta_{\ln IM}$	$\mu_{\ln IM}$	$\beta_{\ln IM}$
Adobe	Adobe	1–2	[§]	-	-	0.2	-	-	0.10	0.48	0.22	0.44	0.26	0.47	0.28	0.56
Unreinforced Masonry, Low-Rise	URM-LR	1–2	[§]	-	-	0.2	-	-	0.12	0.35	0.29	0.30	0.36	0.39	0.40	0.48
Unreinforced Masonry, Mid-Rise	URM-MR	3–5	[§]	-	-	0.5	-	-	0.12	0.37	0.23	0.31	0.29	0.37	0.34	0.49
Steel frame, No-Code, Low-Rise	SMF-NC-LR	1–2	2a[§]	1.0-1.1	1.25-1.35	0.3	-	1.9	0.28	0.66	0.38	0.58	0.48	0.55	0.60	0.55
Steel frame, Mid-Code, Low-Rise	SMF-MC-LR	1–2	7a	1.1-1.2	1.25-1.35	0.3	5.0,7.5	2.4	0.42	0.57	0.65	0.54	0.81	0.55	0.93	0.58
Steel frame, High-Code, Low-Rise	SMF-HC-LR	1–2	3a	1.2-1.3	1.25-1.35	0.3	5.0,7.5	3.0	0.28	0.60	0.76	0.55	1.25	0.56	1.62	0.56
Steel frame, No-Code, Mid-Rise	SMF-NC-MR	3–5	2a	1.0-1.1	1.30-1.40	0.7	-	1.7	0.12	0.34	0.16	0.30	0.21	0.31	0.27	0.32
Steel frame, Mid-Code, Mid-Rise	SMF-MC-MR	3–5	7a	1.1-1.2	1.30-1.40	0.7	5.0,7.5	2.1	0.30	0.57	0.48	0.54	0.60	0.52	0.71	0.53
Steel frame, High-Code, Mid-Rise	SMF-HC-MR	3–5	3a	1.2-1.3	1.30-1.40	0.7	5.0,7.5	2.6	0.34	0.50	0.95	0.46	1.26	0.51	1.44	0.52
Steel frame, No-Code, High-Rise	SMF-NC-HR	≥6	2a	1.0-1.1	1.35-1.45	1.0	-	1.5	0.08	0.37	0.12	0.36	0.16	0.33	0.19	0.29
Steel frame, Mid-Code, High-Rise	SMF-MC-HR	3–5	7a	1.1-1.2	1.35-1.45	1.0	5.0,7.5	1.9	0.21	0.68	0.37	0.66	0.49	0.61	0.65	0.65
Steel frame, High-Code, High-Rise	SMF-HC-HR	3–5	3a	1.2-1.3	1.35-1.45	1.0	5.0,7.5	2.3	0.26	0.65	0.77	0.64	1.31	0.75	2.01	0.84
Steel braced frame, Low-Rise	SBF-MC-LR	1–2	4a	1.2-1.3	1.15-1.25	0.2	3.5,5.5	2.5	0.22	0.58	0.37	0.58	0.57	0.62	0.78	0.58
Steel braced frame, Mid-Rise	SBF-MC-MR	3–5	4a	1.3-1.4	1.20-1.30	0.3	3.5,5.5	2.2	0.23	0.62	0.40	0.55	0.57	0.55	0.80	0.56
Steel braced frame, High-Rise	SBF-MC-HR	≥6	4a	1.4-1.5	1.25-1.35	0.5	3.5,5.5	2.0	0.26	0.49	0.46	0.50	0.70	0.52	0.91	0.54
RC frame, No-Code, Low-Rise	RCF-NC-LR	1–2	2a+*inf* [§§]	1.0-1.1	1.25-1.35	0.2	-	1.9	0.39	0.78	0.46	0.73	0.51	0.73	0.57	0.77
RC frame, Mid-Code, Low-Rise	RCF-MC-LR	1–2	7a+*inf*	1.1-1.2	1.25-1.35	0.2	5.0,7.5	2.4	0.48	0.71	0.56	0.72	0.67	0.82	0.86	0.89
RC frame, High-Code, Low-Rise	RCF-HC-LR	1–2	3a+*inf*	1.2-1.3	1.25-1.35	0.2	5.0,7.5	3.0	0.37	0.76	0.68	0.72	1.03	0.79	1.52	0.86
RC frame, No-Code, Mid-Rise	RCF-NC-MR	3–5	2a+*inf*	1.0-1.1	1.30-1.40	0.5	-	1.7	0.22	0.50	0.25	0.52	0.29	0.52	0.32	0.53
RC frame, Mid-Code, Mid-Rise	RCF-MC-MR	3–5	7a+*inf*	1.1-1.2	1.30-1.40	0.5	5.0,7.5	2.1	0.38	0.57	0.51	0.66	0.61	0.70	0.74	0.72
RC frame, High-Code, Mid-Rise	RCF-HC-MR	3–5	3a+*inf*	1.2-1.3	1.30-1.40	0.5	5.0,7.5	2.6	0.50	0.57	1.01	0.72	1.56	0.80	2.47	0.88
RC frame, Mid-Code, High-Rise	RCF-MC-HR	≥6	7a+*inf*	1.1-1.2	1.35-1.45	0.7	5.0,7.5	1.9	0.37	0.67	0.51	0.65	0.64	0.66	0.78	0.71
RC frame, High-Code, High-Rise	RCF-HC-HR	≥6	3a+*inf*	1.2-1.3	1.35-1.45	0.7	5.0,7.5	2.3	0.44	0.59	0.94	0.61	1.33	0.64	1.70	0.63
RC frame-wall, Mid-Code, Mid-Rise	RCWF-MC-	3–5	7a+4a[†]	1.1-1.2	1.15-1.25	0.3	6.0,7.5	2.5	0.29	0.65	0.83	0.57	1.37	0.58	1.89	0.58
RC frame-wall, High-Code, Mid-Rise	RCWF-HC-MR	3–5	3a+4a	1.2-1.3	1.15-1.25	0.3	6.0,7.5	2.5	0.44	0.55	2.41	0.59	3.14	0.47	3.59	0.44
RC frame-wall, Mid-Code, High-Rise	RCWF-MC-HR	≥6	7a+4a	1.1-1.2	1.20-1.30	0.7	6.0,7.5	2.0	0.21	0.50	0.62	0.47	0.93	0.44	1.20	0.50
RC frame-wall, High-Code, High-	RCWF-HC-HR	≥6	3a+4a	1.2-1.3	1.20-1.30	0.7	6.0,7.5	2.0	0.28	0.48	1.44	0.50	1.81	0.42	2.00	0.40

[§] 2a, 3a, 4a and 7a represent the backbone curves described by standard springs as proposed by FEMA-440a. See Table 2 for definition of the backbone curves. The backbone shapes for Adobe and URM are adopted from Lagomarsino and Giovinazzi (2006).

[§§] *inf* represents an infill SDOF backbone (infill #1 in Dolšek and Fajfar (2008)). It is combined with the backbone curves of "2a", "7a" and "3a" to create capacity curves for infilled frames. See Table 2 for the backbone curve.

[†] Two springs representing frame and wall are combined to create a dual wall-frame system, assuming both contribute equally to the system strength.

[¶] Γ represents the first mode of vibration participation factor adopted, but modified, from Miranda and Taghavi (2005) and FEMA356 (2000).

[¶¶] Coefficient of Distortion (COD), defined as the ratio of peak inter-story drift ratio and peak roof drift ratio adopted, but modified, from previous studies (Aschheim et al. 2007; Gupta and Krawinkler 2000; Katsanos and Vamvatsikos 2017; Xue and Wu 2006). Note that for LR classes with one story, a_{COD} =1.0.

[♦] R is the behavior factor adopted from Standard 2800.

[‡] T^* is the conditioning oscillator period. $Sa(T^*)$ is used for record selection and response prediction (see Section 4.2).

[♣] Ω_o is the over-strength factor inferred from Standard 2800.

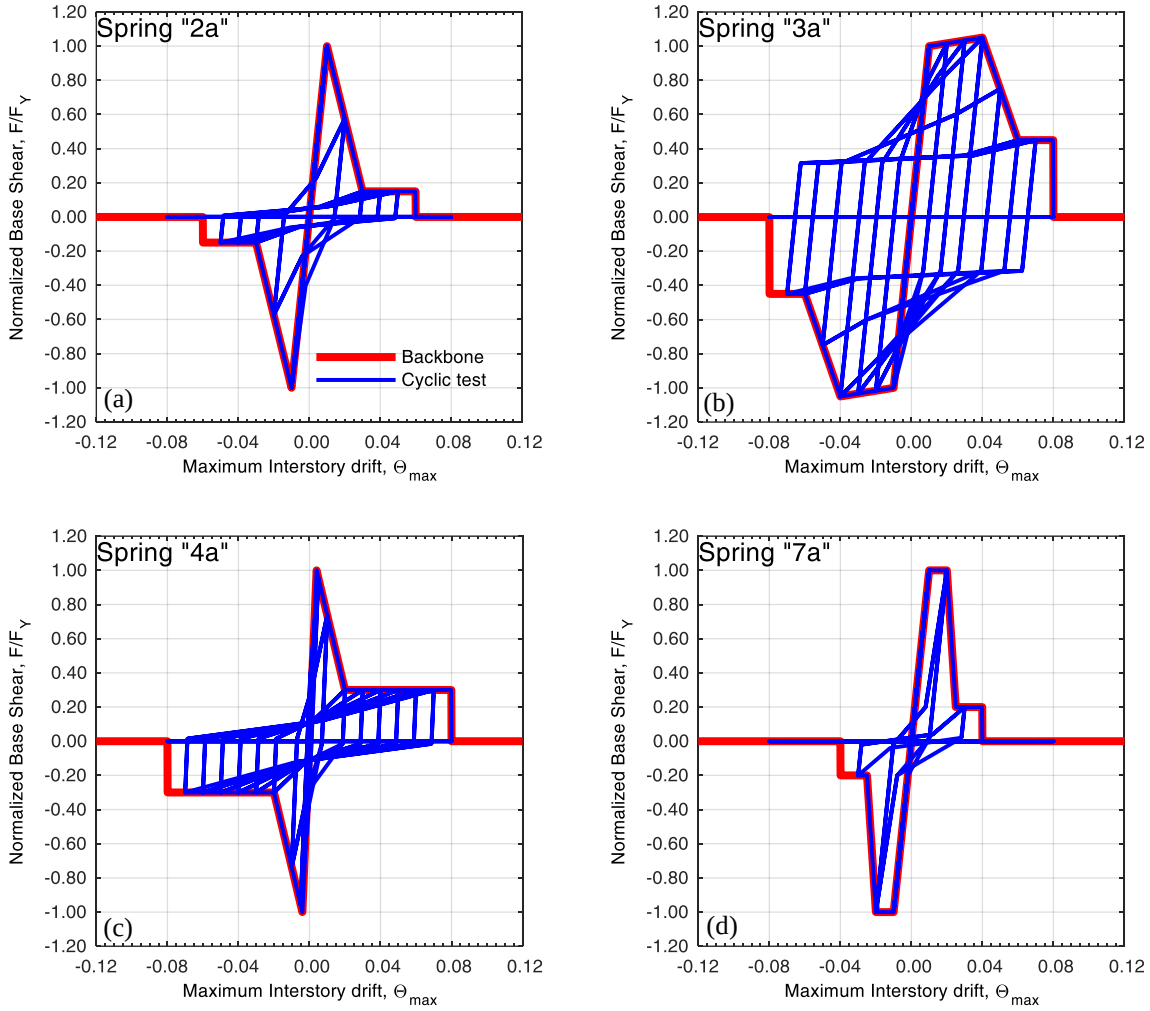

Figure 6. Capacity curves and hysteretic behavior of the four FEMA440a (2009) equivalent SDOF systems adopted to model steel and RC buildings: (a) Non-ductile moment frame (Spring "2a"); (b) Ductile moment frame (Spring "3a"; (c) Stiff non-ductile system for shear walls or braced frames (Spring "4a"); and (d) Limited-ductility moment frame (Spring "7a").

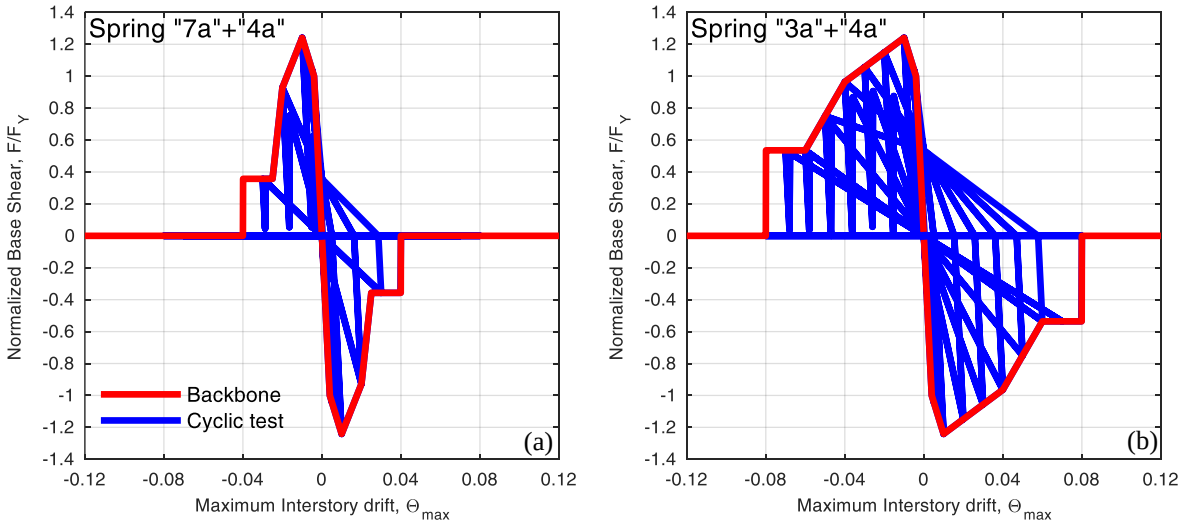

Figure 7. Capacity curves and hysteretic behavior of two compound FEMA440a (2009) equivalent SDOF systems adopted to model dual RC frame-wall systems (a) Mid-Code ("7a"+"4a"); and, (b) High-Code ("3a"+"4a").

On the other hand, the High-Code classes are assumed to benefit from both sufficient strength and ductility capacity. Therefore, we used the backbone curve of a "ductile moment frame", i.e. spring "3a" from FEMA-440a (Figure 6b). The "stiff non-ductile" backbone of spring 4a was taken to represent the behavior of concentric-braced frames and shear walls. For dual wall-frame RC building classes we combined in parallel the capacity curves (springs "7a" or "3a") for moment frames with that of spring 4a for shear walls, essentially contributing 50% each to the global system strength.

To determine the nominal yield base shear of seismically designed buildings (Mid- or High-Code), we follow the design process of Standard 2800, which is similar to that of Eurocode8 (2004) and ASCE7 (2016), by mandating both *strength* and *stiffness* criteria. The strength criterion is based on the elastic design spectrum, the relevant behavior or strength reduction factor, and the over-strength that invariably creeps into realistic designs. The yield base shear, V_y, is thus taken to be equal to $V_y = V_{design} \cdot \Omega_o$. Equivalently, the yield value of the first-mode spectral acceleration at the system's damping is $Sa_y = V_{design} \cdot \Omega_o / W$, where Ω_o is the over-strength factor, W is the total seismic weight of the building and V_{design} is the design base shear stipulated by the code. Based on Standard 2800, $V_{design} = (AB \cdot I/R) \cdot W$, where AB is the reference elastic design spectral acceleration value normalized by g, I is the importance factor (assumed equal to one for the vast majority of ordinary buildings) and R is the behavior factor. To determine AB from the design spectrum we employed the approximate period equations supplied by the code, as a practicing engineer would do. Note that following updates of the seismic code, the design spectrum changes with the year of construction (see Figure 2b). With reference to Figure 2b, only one design spectrum is considered for the Mid-code building classes (corresponding to the very first edition of Standard 2800), while for the High-code classes there are three design spectra (two being actually identical) to choose from. Among these three options, one is randomly selected in proportion to the number of buildings constructed in each time interval of the High-code era extracted from the Census data. Sa_y can, therefore, be simply estimated as $Sa_y = (ABI/R) \cdot \Omega_o$ for the code-based designed buildings. We call this the building *strength* design criterion imposed by the code. The values of Ω_o and R (shown in Table 3) are inferred from Standard 2800 for the systems considered here. Note that in some building classes two R values are reported in Table 3 representing two possible systems in the code corresponding to "intermediate" and "special" frames. Legally, both systems are allowed for Isfahan and therefore, they may have been adopted by different designers. Nevertheless, since according to Standard 2800, Isfahan is classified in a moderate seismicity zone, the "intermediate" systems are probably more widely used. Hence, we weigh here the intermediate systems more than special ones (0.7 versus 0.3) when simulating the family of capacity curves for this class.

The stiffness criterion is based on the Standard 2800 requirement that the maximum inter-story drift ratio along the height of a designed building shall not exceed a limit of θ_{lim}, (e.g., equal to 0.025 for buildings with less than 5 stories, and 0.020 for taller ones in version IV of the code). For flexible buildings, the designers increase the dimensions of the elements to reduce the maximum drift, resulting in larger overall lateral strength and stiffness. To reflect this criterion in our computations for the code-based classes, we estimate the required equivalent SDOF displacement δ_{lim} for a story drift limit of θ_{lim} as:

$$\delta_{\text{lim}} = \frac{\theta_{\text{lim}} \cdot (N_{st} \cdot H_{st})}{\Gamma \cdot a_{\text{COD}}}, \tag{3}$$

Under the two assumptions of (a) constant yield displacement δ_y equal to that computed for the strength criterion as per Aschheim (2002), and (b) equal displacement (or elastic behavior) holding at the design level earthquake, the yield base shear required to limit the design-load-level displacement to δ_{lim} is equal to $V_y = V_{design} \cdot \delta_y / \delta_{\text{lim}}$. By introducing Eq. (3) and replacing V_{design} by the code mandated value, we can estimate the stiffness-required yield base shear as

$$V_y = \frac{\Gamma \cdot AB \cdot I \cdot a_{\text{COD}} \cdot W \cdot \delta_y}{\theta_{\text{lim}} \cdot N_{st} \cdot H_{st}}, \tag{4}$$

Some small over-strength factor could also be incorporated, but lacking data it is taken as 1.0 for satisfying the stiffness criterion. Finally, as the overall actual strength of the equivalent SDOF we adopted the larger V_y value out of the two obtained by enforcing both the *strength* and the *stiffness* criteria. To generate the 100 realizations of the backbone curves, the values of the inelastic displacement parameters on the central backbone curve (e.g., the coordinate of the points C, D, E, F and G in Figure 5b) were randomly sampled from a uniform distribution between 0.8–1.2 of their central values. No additional strength uncertainty is incorporated beyond what is assumed due to its elastic design properties. Some higher variability should actually be expected in practice, rendering several buildings less than code worthy. However, at this time there is too little data for us to reliably quantify this effect.

4.1.4. Infills

RC frame buildings in Isfahan are commonly built with masonry infill walls. The infills can significantly affect the overall seismic behavior of RC buildings. They commonly increase the initial stiffness and lateral strength of the system; after they fail, their impact abruptly drops and the system eventually becomes a bare frame (Dolšek and Fajfar 2008; Matjaž and Peter 2005; Uva et al. 2012). To account for this effect, we followed the approach proposed in Dolšek and Fajfar (2008) to combine the equivalent SDOF capacity curves of RC "bare frames" with "infills" by placing their springs in parallel. The backbone capacity curve utilized for the infills is shown in Table 2. Based on previous findings such as Repapis et al. (2006) and O'Reilly and Sullivan (2018), we assumed a ratio between peak strength of the infilled frame over the peak strength of bare frames equal to 2.0, 1.5 and 1.5 for NC, MC and HC RC frames, respectively. This is because the presence of infills in old non-ductile frames significantly increases the overall initial stiffness and strength of the building while this effect is, relatively speaking, reduced for the stronger, newer MC and HC frames. This infill strength is considered in addition to the "code-based" base shear capacity of the systems, calculated as per the previous section, as infill strength is never accounted for in practical design. The effect of infills was neglected for the dual wall-frame systems assuming, as typical, that the stiffness and strength of RC walls dominate over the amounts contributed by the infills.

4.1.5. Elastic, modal and geometric properties

The adopted values of N_{st}, Γ, a_{COD}, for each building class are listed in Table 3. 100 equivalent SDOF backbone realizations of each building class are generated by sampling building characteristics from the distributions adopted for each class. For example, the number of stories, Γ and a_{COD} are uniformly generated within the ranges reported in Table 3. The range for Γ is based on the recommendations of Miranda and Taghavi (2005) and FEMA356 (2000), while a_{COD} bounds are inferred from multiple studies (Aschheim et al. 2007; Gupta and Krawinkler 2000; Katsanos and Vamvatsikos 2017; Xue and Wu 2006). Due to its relatively minor variation and low influence, we considered a constant story height H_{st}=2.6m for the URM and adobe building classes based on the work of Villar-Vega et al. (2017) for South America and H_{st}=3.2m for the rest of the classes according to Sadeghi et al. (2015). A damping ratio, ξ, equal to 5% is considered for RC and masonry buildings, while a lower value equal to 2% is employed for steel structures, as welded connections are commonly used in Isfahan. Note that the variability in the parameters is based on judgment; having empirical data would allow a more informed selection similarly to what is done in Silva et al. (2015). Figure 8a shows the 100 realizations of the backbone curves generated for the "SMF-HC-MR" building class together with the original central backbone curve, normalized by their yield strength. Figure 8b shows the same 100 realizations and the mean and mean +/-σ capacity curves in terms of roof displacement versus the yield base shear coefficient C_y.

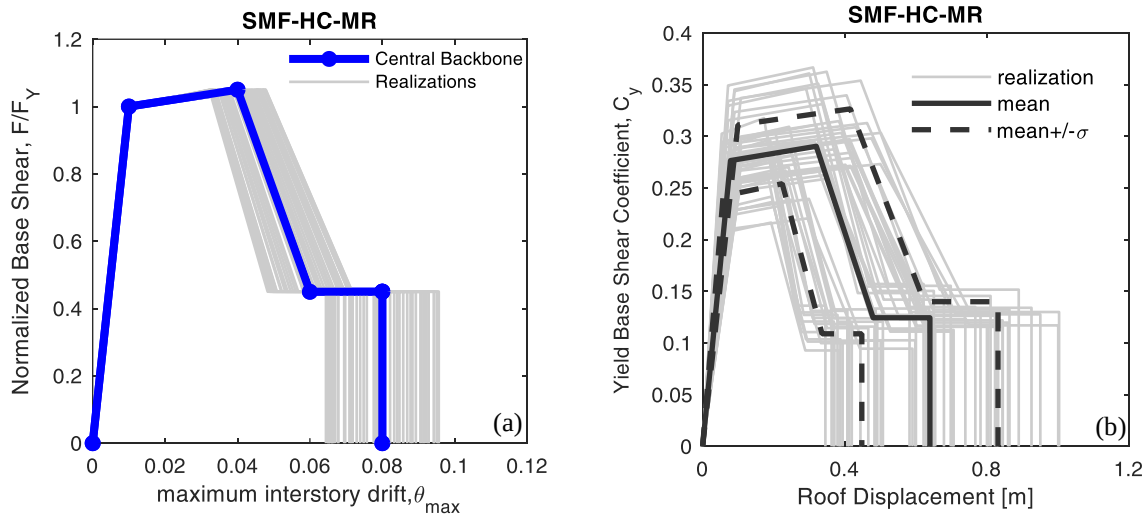

Figure 8. a) Illustration of normalized backbone curve for "SMF-HC-MR" building class and 100 realizations; b) Capacity curves, i.e., 100 realizations, mean and mean +/- one standard deviation (σ) for the "SMF-HC-MR" building class.

4.2 Ground motion selection

Multiple Stripe Analysis, MSA, (Jalayer and Cornell 2009) is performed to estimate the response of the equivalent SDOFs using a large database of natural ground motion recordings. This requires multiple nonlinear dynamic analyses at each of several predetermined levels of the IM. To accurately capture the site-hazard-dependence of fragility and vulnerability curves (Kohrangi et al. 2017), appropriate record selection is required at each IM level

to provide the link between the site hazard and structural response. Herein we utilize the conditional-spectrum (CS) record selection approach (Jayaram et al. 2011) to select sets of records that best represent the seismic hazard in Isfahan. Twelve levels of ground shaking intensity are considered, corresponding to probabilities of exceedance of 70%, 50%, 10%, 7.5%, 5%, 4%, 2%, 1%, 0.75%, 0.5%, 0.2% and 0.1% in 50 years. The IM of choice is the 5%-damped geomean spectral acceleration of the two horizontal components, $Sa(T^*)$, determined at the five oscillator periods of T^*=0.2, 0.3, 0.5, 0.7 and 1.0s, as listed in Table 3 for the different classes of buildings. These conditioning periods are selected close to the fundamental periods, T_1, of the systems to increase the *efficiency* in response prediction and, thus, to achieve a lower uncertainty in the response and loss estimates (Luco and Cornell 2007).

We performed hazard and disaggregation analyses for a site in the center of the city with Vs_{30}=400 m/s, a value that is considered to describe an average common soil type for the entire city. We used the EMME14 hazard source model (Şeşetyan et al. 2018) and the OpenQuake software (Silva et al. 2014a) to perform the hazard analysis. More details about the model and the probabilistic seismic hazard analysis (PSHA) are provided in the companion paper (Kohrangi et al. 2020). Disaggregation analysis is performed to identify the scenarios most contributing to the hazard for each of the five conditioning periods and for each of the 12 intensity (or probability of exceedance) levels. As an example, Figure 9a shows the disaggregation results for Sa(0.5s) at IM level 5 corresponding to a probability of exceedance of 4% in 50 years. The mean scenario (i.e., mean magnitude and mean distance from rupture) for one GMPE branch of the logic tree corresponding with ASK14 for strike-slip faulting (Abrahamson et al. 2014) was used to generate the "approximate" CS target spectrum (Lin et al. 2013). For each IM level, 21 records from the PEER NGA West database (Chiou et al. 2008) caused by crustal fault events are selected and scaled to collectively match the target geomean spectral acceleration mean and variance. From each recording, a single horizontal component is chosen at random leading to a total of 252 ordinary (i.e., non-pulse-like, not long duration) ground motion records per IM type. Figure 9b shows the CS and the response spectra of a set of 21 ground motion records for Sa(0.5s) at a probability of exceedance of 4% in 50 years.

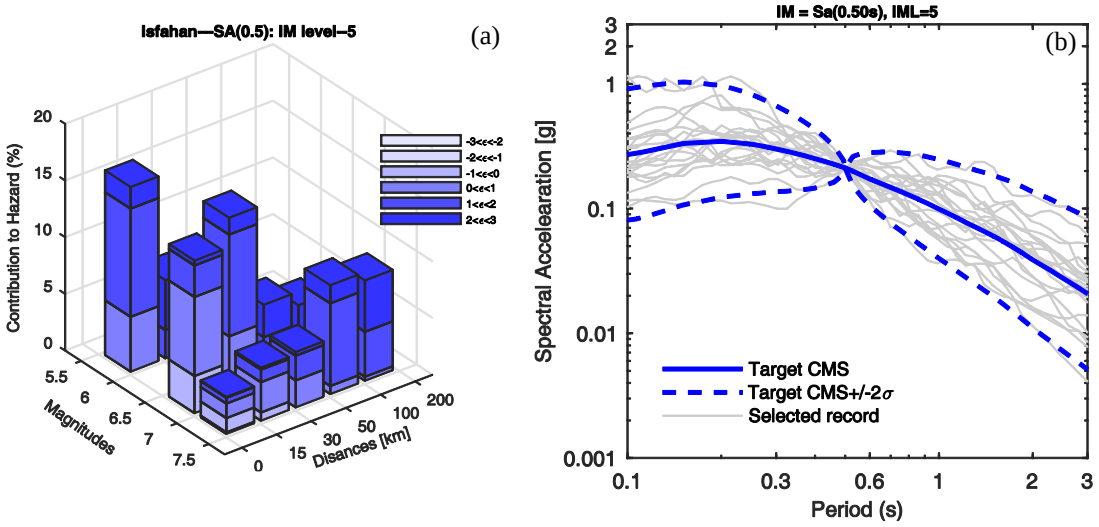

Figure 9. Record selection details for IM=Sa(0.5s) at IM level 5 corresponding to a probability of exceedance of 4% in 50 years; a) Disaggregation results showing the contribution of each scenario to the hazard, where epsilon (ε) shows the number of standard deviations from the logarithmic mean of the IM for a specific GMPE (Baker and Cornell 2006); b) CS-based record selection, showing the 2.5/50/92.5th target percentiles of the spectral acceleration (CMS denoting the 50th percentile) and the spectra of 21 records selected to statistically match them.

4.3 Damage classification, consequence functions and vulnerability curves

Four building global damage states are considered corresponding to *slight*, *moderate*, *extensive* and *collapse* level damages. These damage states are defined on the basis of the capacity curve of each system. In general the recommendations of previous studies (Silva et al. 2014b; Villar-Vega et al. 2017) were followed to determine the engineering demand parameter (EDP) threshold at the onset of each damage state. Clearly this is an imperfect assumption, given the lack of better data, based only on matching the macro characteristics of building classes. This EDP threshold here is expressed in terms of the maximum inter-story drift, rather than the typical roof drift. We contend that our approach offers a more realistic basis for damage determination, consistent with state-of-the-art guidelines for single building loss assessment (FEMA-P58 2012) that prefer local rather than global EDPs to measure response. Herein slight damage corresponds to 75% of the yield drift (θ_s), while collapse happens at a

drift where the lateral strength is reduced to 80% of its maximum value (referred to as the ultimate drift, θ_u). Consequently, the moderate and extensive damage states are defined at drift values of $\theta_s+0.3\cdot(\theta_u-\theta_s)$ and $\theta_s+0.6\cdot(\theta_u-\theta_s)$, respectively, tri-secting the interval between slight damage and collapse.

For each building class nonlinear dynamic analyses are conducted at the 12 IM levels for 21 records each and for all the 100 realizations of the equivalent SDOF's backbones to quantify the distribution of the maximum displacement and inter-story drift response and estimate the probability of exceeding each damage state conditional on the IM level. The results are sets of 12×21×100 data points per building class and damage state that can be employed to fit corresponding lognormal fragility curves using the maximum likelihood method (Baker 2015). The resulting fragility parameters, i.e., the logarithmic mean, $\mu_{\ln IM}$, and standard deviation, $\beta_{\ln IM}$, obtained for four damage states and for all of the building classes are reported in the last columns of Table 3, while an example appears in Figure 10a for the "RCF-HC-MR" building class. Figure 10a depicts 100 realizations of the fragility curves for four damage states (in grey lines) as well as the final aggregated fragility curves (in colored lines). Note that no overlapping of individual fragility realizations in consecutive limit-states seems to occur. This observation is due to the high ductility and consequent good separation among limit-states for this high-code class; it should not be extended to less ductile building classes.

The aggregated curves are not single-building fragility curves but rather single-class fragility curves that are simultaneously accounting for both the building-to-building and the record-to-record variability in Isfahan. Their advantage is that they are offering a simple representation of an entire set of same-class structures anywhere in Isfahan and they are fully appropriate for an urban level risk assessment study such as this one. However, in some respect this is also their greatest disadvantage, as they somewhat hide the individual contributions of salient members of each class and in some cases their use may introduce some bias in the final results. For example, as mentioned earlier, Miranda and Heresi (2018) have observed that one-story buildings systematically experience lower loss ratios than those of similar two-story buildings. This effect is hidden inside a family of fragility curves for a class of buildings; if the fragility curves for one-story and two-story buildings for a given class are not weighted by their proportions in the overall building stock, some potential bias may creep into the final loss estimates.

In this study, class-fragility curves will not be directly employed to determine the loss, but only the statistics of buildings in each damage state after any event throughout the city of Isfahan. To develop vulnerability functions and to estimate losses we employ the individual building-fragility curves instead, one for each of the 100 realizations per class. To do so we fit individually the 12×21 data points for each case to obtain a set of 100 fragility curves per class. This family may aggregate to the same class-fragility curve estimated earlier, but it allows for higher resolution computations and offers accurate propagation of uncertainty to the vulnerability estimates.

In general, as mentioned earlier, consequence models (or functions) are used to convert a set of fragility functions into vulnerability functions. Such models show the distribution of the fraction of loss (i.e., the cost of repair to the cost of replacement or number of injuries/fatalities to the total number of residents in the building) estimated to occur when a structure is in any given damage state after an earthquake. The most defensible way to derive these functions is from repair costs from insurance claims submitted by householders after the occurrence of an earthquake or from the number of fatalities in the same (or a similar) region for each class of building. Despite the occurrence of large number of earthquakes in recent years in Iran, to the best of the authors' knowledge country-specific consequence functions are not available in the literature. For this reason, herein we make use of consequence models developed for other regions (Bal et al. 2008; Di Pasquale and Goretti 2001; FEMA-443 2003; Kappos et al. 2006). We are, however, fully aware that these models may be based on different definitions of damage states and may incorporate local practices, costs and policies that should be carefully evaluated when they are utilized in a different region.

Given the similarity of the damage states considered in this study with the ones defined in Silva et al. (2015), we use the latter consequence model with 0.1, 0.3, 0.6 and 1.0 as the mean relative cost ratios for slight, moderate, extensive and collapse damage states, respectively. For simplicity, no additional uncertainty distribution was considered for the cost ratios. For each single-building fragility curve obtained from a specific equivalent SDOF realization, this consequence function was used to derive the corresponding single-building vulnerability curve. Figure 10b shows the 100 realizations of the vulnerability curves (in grey) obtained for the "RCF-HC-LR" class using the fragility curves in Figure 10a and the consequence function just discussed. The loss ratio in these realizations is assumed to follow a lognormal distribution given the IM. As the lognormal is unbounded on the right tail, loss ratios greater than 1.0 are truncated to the total loss of 1.0. The mean curve, together with its variability, provide the final vulnerability function for that building class.

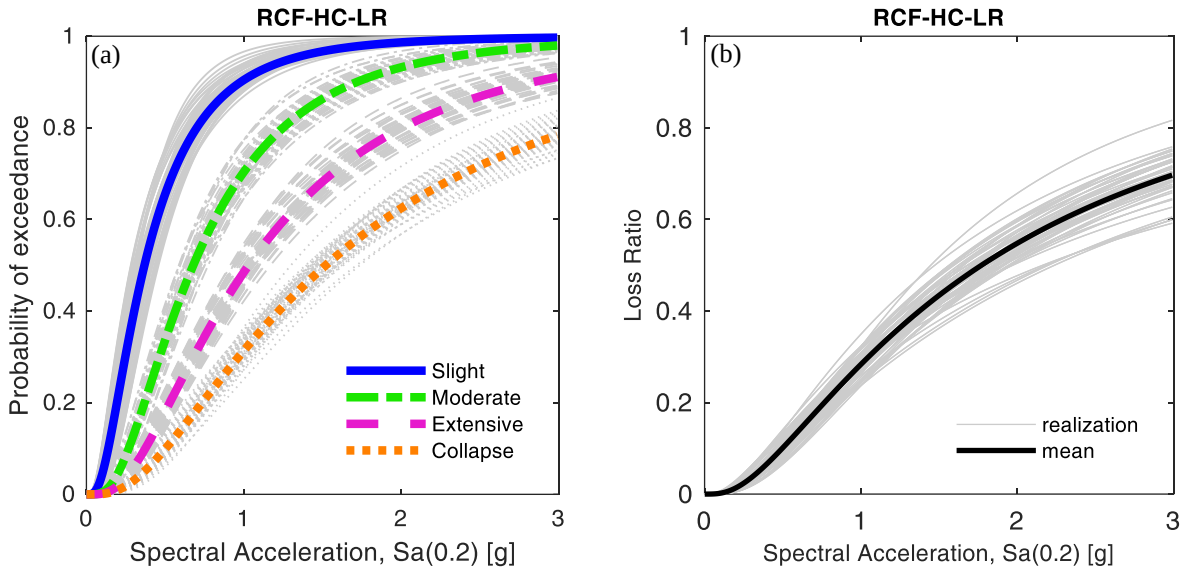

Figure 10. (a) Fragility curves for different damage states developed for the "RCF-HC-LR" building class. The grey lines show the curves obtained from different realizations; and (b) mean vulnerability curve (in black) and the corresponding 100 realizations resulting for the "RCF-HC-LR" class.

For illustration purposes, Figure 11 shows a comparison between resulting mean vulnerability curves that use the same conditioning IMs of *Sa*(0.2s) in the left panel and *Sa*(0.5s) in the right panel, i.e., stiff low-rise and stiff mid-rise structures, respectively. As expected, the Adobe and URM are the most vulnerable low-rise buildings, while the RC structures designed by the latest versions of the seismic design code are the least vulnerable low/mid-rise ones, at least when stiff low-period structures are considered (i.e., no steel frames). Figure 12 instead compares our vulnerability curves for two building classes in Isfahan with the corresponding ones proposed by Sadeghi et al. (2015) for the entire Iran and by Villar-Vega et al. (2017) for the entire South America. Sadeghi et al. (2015) directly provides vulnerability curves in terms of PGA, which we approximately translated into *Sa*(0.2s) and *Sa*(0.5s) by using the PGA to *Sa* ratio extracted from the Uniform Hazard Spectrum at 10% in 50yrs developed using the EMME model for Isfahan. Note that Villar-Vega et al. (2017) provided only fragility curves that we convolved with the same consequence function employed herein to obtain the vulnerabilities curves displayed in the figure.

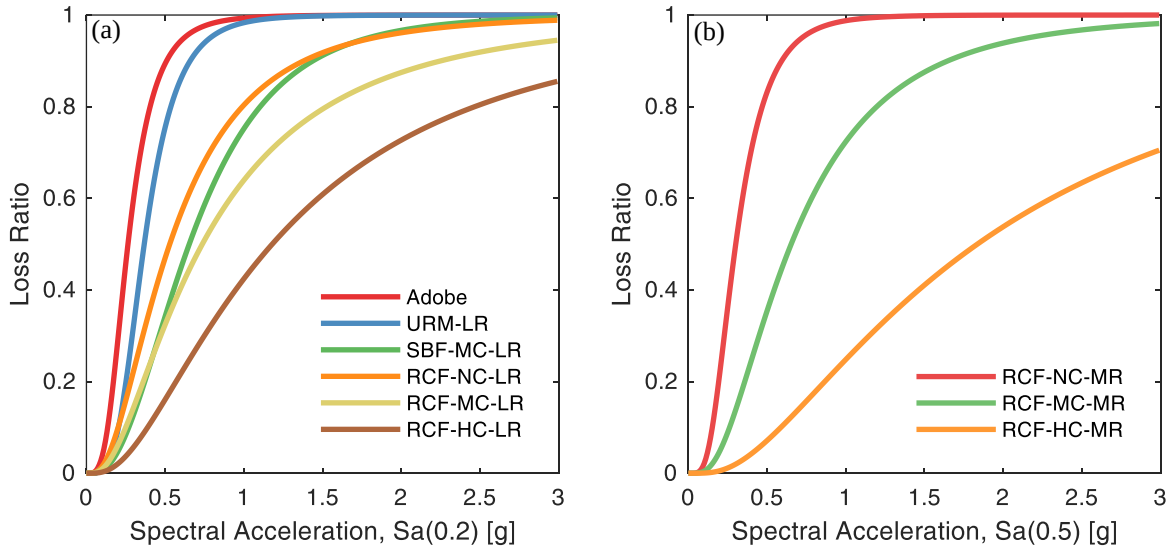

Figure 11. Comparison of the mean vulnerability curves among different building classes that share the same conditioning IM: a) $Sa(T^*=0.2s)$, b) $Sa(T^*=0.5s)$.

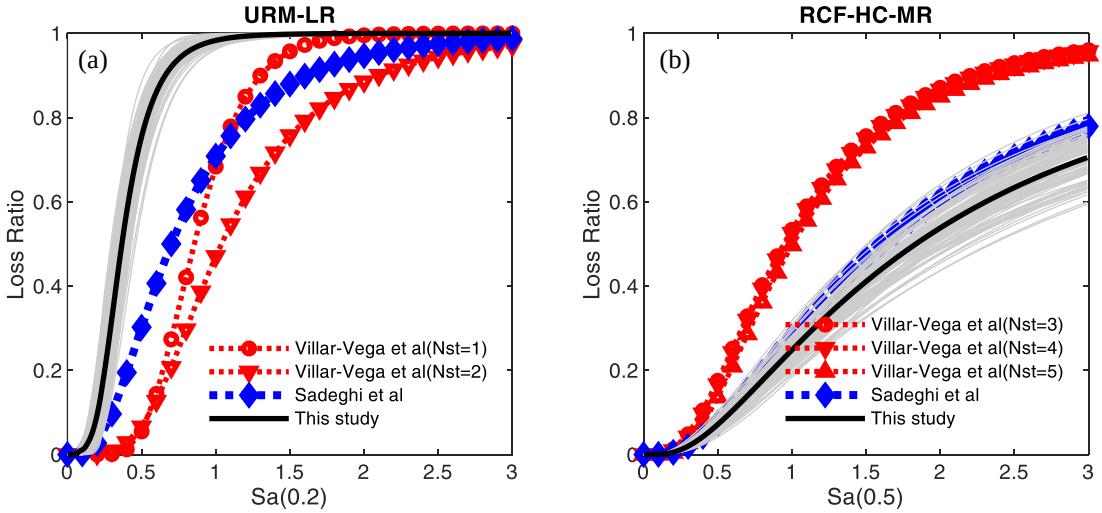

Figure 12. Comparison of our proposed vulnerability curves with those of Villar-Vega et al. (2017) and Sadeghi et al. (2015) for the "URM-LR" and "RCF-HC-MR" building classes.

Overall, for RC buildings our vulnerability curves in general are fairly close to those of Sadeghi et al. (2015) for the all High Code cases (nearly identical for the High-Code Mid-Rise RC frames case shown in Figure 12b) while they appear to be lower than those of Villar-Vega et al. (2017). However, our proposed vulnerability curves diverge significantly compared to both studies for all the No Code cases, as also shown in Figure 12a for URM low-rise buildings. In general, we are predicting more damage at lower intensities for Isfahan than the vulnerability from previous studies would. Since the low code and URM buildings comprise most of the building stock, this implies that our estimates will tend towards higher losses vis-à-vis, for example, those that could be computed using the vulnerability curves of Sadeghi et al. (2015).

In order to estimate the number of casualties (i.e., fatalities or injuries) in a seismic event, it is necessary to establish a relation between any structural damage state used in the fragility models and the percentage of casualties among the occupants. For each building class, human loss vulnerability curves are also considered based on the recommendations of Spence (2007). This study defines the percent of injured occupants for different classes of buildings and for six different severity levels of injury ranging from uninjured (UI) to death (I_5). Table 4 shows the suggested values for different building types. It should be noted that, based on this study, the injuries and fatalities happen only when the building collapses. This assumption appears un-conservative and should be revised in future studies. Therefore, given the assumption above, the human loss curves per each of the six injury levels are simply obtained as the product of the collapse fragility curve of each building class with the constant values suggested in Table 4.

Table 4. Injury distributions for specific building types that collapsed adopted from Spence (2007). (Note: UI, uninjured; I_1, slight injuries; I_2, moderate injuries; I_3, serious injuries; I_4, critical injuries; I_5, deaths).

Building Type	UI (%)	I_1 (%)	I_2 (%)	I_3 (%)	I_4 (%)	I_5 (%)
Masonry						
1 storey	23.6	50.0	12.0	8.0	0.4	6.0
2-3 storeys	16.5	50.0	15.0	10.0	0.5	8.0
>4 storeys	9.4	50.0	18.0	12.0	0.6	10.0
RC						
1 storey	32.9	30.0	19.0	3.0	0.2	15.0
2-3 storeys	20.8	30.0	23.0	4.0	0.2	22.0
>4 storeys	9.7	30.0	27.0	5.0	0.3	28.0
Steel						
1 storey	38.9	30.0	15.0	2.0	0.1	14.0
2-3 storeys	25.1	30.0	19.0	3.0	0.2	22.8
>4 storeys	10.0	30.0	23.0	4.0	0.2	32.8

5. Concluding remarks

This paper presents the first part of the seismic risk assessment of Isfahan, Iran, and focuses on exposure, fragility and vulnerability of ordinary structures. A comprehensive residential, mixed residential/commercial and public

building taxonomy is developed for the Iranian stock based on the 2011 Census data together with local surveys resulting in a total of 27 building classes based on different material/lateral-load-resisting system, age and height. The total estimated replacement cost of the entire residential building stock is 26.21 billion Euro. To characterize the seismic response and, therefore, the performance of each building class, we utilized a generalized equivalent single degree of freedom system with a parameterized backbone curve and a hysteresis behavior that match those expected for structures in each class. Empirical data and engineering judgement are both employed to determine the distribution of the backbone curve parameters for pre-standard eras. For more recent structures to estimate the system parameters we adopted instead a simplified design process that followed the prescriptions of the codes applicable in those years. Hazard consistent ground motions are selected and nonlinear dynamic analysis is employed to derive class- and site-specific fragility and vulnerability curves for all the building classes in the greater area of Isfahan. This exposure model together with these fragility/vulnerability functions are then used in the risk model for Isfahan discussed in the companion paper (Kohrangi et al. 2020).

These two modules were developed according to state-of-the-art approaches. However, in hindsight, many assumptions needed to be made because of the scarcity of information regarding especially the construction quality and building loss values. In an urban risk study, such as the one pursued here, no particular regard has been devoted to the numerous cultural heritage buildings in Isfahan. These historical buildings, due to their unique characteristics and immeasurable value to the community, would require a case-specific treatment that is beyond our scope.

6. Acknowledgement

The first author is grateful for the financial support provided by the Iranian National Elites Foundation and by the Scuola Universitaria Superiore IUSS Pavia. Additional financial support has been provided by the Executive Agency for Small and Medium-sized Enterprises (EASME) under the powers delegated by the European Commission through the Horizon 2020 program “HYPERION- Development of a decision support system for improved resilience & sustainable reconstruction of historic areas to cope with climate change & extreme events based on novel sensors and modelling tools”, Grant Agreement number 821054. We thank Dr. Hossein Tajmir Riahi for his kind help and insightful suggestions in the process of exploring the building stock data for Isfahan. We also thank the Municipality of Isfahan and the related sectors of Isfahan Municipality ICT Organization and Urban Development and Architecture Assistance for providing the GIS-based data of 2011 Census to be used within the scope of this study.

7. References

Abrahamson NA, Silva WJ, Kamai R (2014) Summary of the ASK14 Ground Motion Relation for Active Crustal Regions Earthquake Spectra 30:1025-1055 doi:10.1193/070913eqs198m

Alavi E, Mahootchian A, Yadegari S, Shamsodin M, Babania Nouri M, Ordoubadi B (2018) Report of M7.3 Ezgele, Kermanshah, Iran Earthquake on November 12, 2017, EERI reports.

ASCE7 (2016) Minimum Design Loads for Buildings and Other Structures. Reston, VA

Aschheim M (2002) Seismic Design Based on the Yield Displacement Earthquake Spectra 18:581-600 doi:10.1193/1.1516754

Aschheim M, Maurer EP, Browning J (2007) Dependency of COD on ground motion intensity and stiffness distribution Structural Engineering and Mechanics 27:425–438

Aslani H, Cabrera C, Rahnama M (2012) Analysis of the sources of uncertainty for portfolio-level earthquake loss estimation Earthquake Engineering & Structural Dynamics 41:1549-1568 doi:doi:10.1002/eqe.2230

Baker J, Cornell C (2006) Spectral shape, epsilon and record selection Earthquake engineering and structural dynamics 35:1077–1095

Baker JW (2015) Efficient Analytical Fragility Function Fitting Using Dynamic Structural Analysis Earthquake Spectra 31:579-599 doi:10.1193/021113eqs025m

Bal İE, Crowley H, Pinho R, Gülay FG (2008) Detailed assessment of structural characteristics of Turkish RC building stock for loss assessment models Soil Dynamics and Earthquake Engineering 28:914-932 doi:https://doi.org/10.1016/j.soildyn.2007.10.005

Bazzurro P, Luco N Accounting for Uncertainty and Correlation in Earthquake Loss Estimation. In: Proceedings of the Ninth International Conference on Structural Safety and Reliability, Rome, Italy, 2005. pp 2687-2694

Bazzurro P, Park J The effects of portfolio manipulation on earthquake portfolio loss estimates. In: Proceedings of the 10th international conference on applications of statistics and probability in civil engineering, Tokyo, Japan, 2007.

Borzi B, Crowley H, Pinho R (2008) Simplified Pushover-Based Earthquake Loss Assessment (SP-BELA) Method for Masonry Buildings International Journal of Architectural Heritage 2:353-376 doi:10.1080/15583050701828178
Chiou B, Darragh R, Gregor N, Silva W (2008) NGA Project Strong-Motion Database Earthquake Spectra 24:23-44 doi:10.1193/1.2894831
D'Ayala D, Meslem A, Vamvatsikos D, Porter K, Rossetto T, Crowley H, Silva V (2014) Guidelines for Analytical Vulnerability Assessment of Low-Mid-Rise Buildings – Methodology. Vulnerability Global Component Project, GEM Foundation, Pavia, Italy.
Di Pasquale G, Goretti A (2001) Vulnerabilità funzionale ed economica degli edifici residenziali colpiti dai recenti eventi sismici italiani. Paper presented at the Proceedings of the 10th national conference "L'ingegneria Sismica in Italia", Potenza-Matera, Italy,
Dolšek M, Fajfar P (2008) The effect of masonry infills on the seismic response of a four-storey reinforced concrete frame — a deterministic assessment Engineering Structures 30:1991-2001 doi:https://doi.org/10.1016/j.engstruct.2008.01.001
Eurocode8 (2004) design of structures for earthquake Resistance. Comité Européen de Normalisation, Brussels, Belgium
Fallah Tafti M, Amini Hosseini K, Mansouri B (2020) Generation of new fragility curves for common types of buildings in Iran Bulletin of Earthquake Engineering 18:3079-3099 doi:10.1007/s10518-020-00811-5
FEMA356 FEMA (2000) Prestandard and Commentary for the Seismic Rehabilitation of Buildings. Washington, D.C, FEMA 356
FEMA440a (2009) Effects of Strength and Stiffness Degradation on Seismic Response. Applied Technology Council, 201 Redwood Shores Parkway, Suite 240, Redwood City, California 94065
FEMA-443 (2003) HAZUS-MH technical manual. Federal Emergency Management Agency. Washington DC, USA
FEMA-P58 (2012) Federal Emergency Management Agency: Seismic Performance Assessment of Buildings, prepared by the Applied Technology Council for the Federal Emergency Management Agency. Washington, DC
Ghayamghamian M, Khanzadeh K (2008) Fragility curves for masonry buildings in Iran. Paper presented at the 1st International Conference on Seismic Retrofitting, , Tabriz, Iran,
Ghodrati Amiri G, Razeghi H, Doosti L (2014) Development of Analytical Fragility Curves for Iran's Masonry school Buildings SHARIF: CIVIL ENINEERING 31:145-156
Goda K, Yoshikawa H (2012) Earthquake insurance portfolio analysis of wood-frame houses in south-western British Columbia, Canada Bulletin of Earthquake Engineering 10:615-643 doi:10.1007/s10518-011-9296-9
Gupta A, Krawinkler H (2000) Estimation of seismic drift demands for frame structures Earthquake Engineering & Structural Dynamics 29:1287-1305 doi:doi:10.1002/1096-9845(200009)29:9<1287::AID-EQE971>3.0.CO;2-B
Hisada Y, Shibayama A, Ghayamghamian M (2005) Building damage and seismic intensity in Bam city from the 2003 Bam earthquake Bull Earthquake Res Inst, Univ Tokyo 79:81–93
Hosseini M, Majd M (2011) Developing fragility curves for regular steel buildings with X-bracing using nonlinear time history Sharif J Civil Eng 27:3–13.
ICSRDB (2014) Iranian Code of Practice for Earthquake Resistant Design of Buildings (Standard 2800), 4th Edition. PN S 253, Building and Housing Research Center of Iran,
Jalayer F, Cornell C (2009) Alternative nonlinear demand estimation methods for probability-based seismic assessments Earthquake Engineering & Structural Dynamics 38:951–972
Jayaram N, Lin T, Baker J (2011) A Computationally Efficient Ground-Motion Selection Algorithm for Matching a Target Response Spectrum Mean and Variance. Earthquake Spectra 27:797-815
JICA (2000) The Study on seismic microzoning of the greater Tehran area in the Islamic Republic of Iran.
Jorge RG, Eduardo M (2007) Probabilistic estimation of maximum inelastic displacement demands for performance-based design Earthquake Engineering & Structural Dynamics 36:1235-1254 doi:doi:10.1002/eqe.680
Kappos AJ, Panagopoulos G, Panagiotopoulos C, Penelis G (2006) A hybrid method for the vulnerability assessment of R/C and URM buildings Bulletin of Earthquake Engineering 4:391-413 doi:10.1007/s10518-006-9023-0
Katsanos EI, Vamvatsikos D (2017) Yield frequency spectra and seismic design of code-compatible RC structures: an illustrative example Earthquake Engineering & Structural Dynamics 46:1727-1745 doi:doi:10.1002/eqe.2877
Kazemi H, Ghafory-Ashtiany M, Azarbakht A (2013) Effect of epsilon-based record selection on fragility curves of typical irregular steel frames with concrete shear walls in Mashhad city International Journal of Advanced Structural Engineering 5:23 doi:10.1186/2008-6695-5-23

Kohrangi M, Bazzurro P, Vamvatsikos D (2020) Seismic risk and loss estimation for building stock in Isfahan. Part II: Hazard analysis and risk assessment Earthquake Spectra (in review)
Kohrangi M, Vamvatsikos D, Bazzurro P (2016) Implications of Intensity Measure Selection for Seismic Loss Assessment of 3-D Buildings Earthquake Spectra 32:2167-2189 doi:10.1193/112215eqs177m
Kohrangi M, Vamvatsikos D, Bazzurro P (2017) Site dependence and record selection schemes for building fragility and regional loss assessment Earthquake Engineering & Structural Dynamics 46:1625-1643 doi:10.1002/eqe.2873
Lagomarsino S, Giovinazzi S (2006) Macroseismic and mechanical models for the vulnerability and damage assessment of current buildings Bulletin of Earthquake Engineering 4:415-443 doi:10.1007/s10518-006-9024-z
Lin T, Harmsen S, Baker J, Luco N (2013) Conditional spectrum computation incorporating multiple causal earthquakes and ground motion prediction models BSSA 103:1103–1116
Luco N, Cornell C (2007) Structure-Specific Scalar Intensity Measures for Near-Source and Ordinary Earthquake Ground Motions Earthquake Spectra 23:357-392
Mansouri B, Ghafory-Ashtiany M, Amini-Hosseini K, Nourjou R, Mousavi M (2010) Building Seismic Loss Model for Tehran Earthquake Spectra 26:153-168 doi:10.1193/1.3280377
Matjaž D, Peter F (2005) Simplified non-linear seismic analysis of infilled reinforced concrete frames Earthquake Engineering & Structural Dynamics 34:49-66 doi:doi:10.1002/eqe.411
Miranda E, Heresi P (2018) Seismic risk comparison between 1- and 2- story houses for performance-based earthquake engineering. Paper presented at the 16th European Conference in Earthquake Engineering, Thessaloniki, 18-21 June,
Miranda E, Taghavi S (2005) Approximate Floor Acceleration Demands in Multistory Buildings. I: Formulation Journal of Structural Engineering 131:203-211 doi:doi:10.1061/(ASCE)0733-9445(2005)131:2(203)
Mitrani-Reiser J (2007) An ounce of prediction: probabilistic loss estimation for performance-based earthquake engineering. Calofornia Institute of Technology.
Moehle JP (1992) Displacement-Based Design of RC Structures Subjected to Earthquakes Earthquake Spectra 8:403-428 doi:10.1193/1.1585688
Mostafaei H, Kabeyasawa T (2004) Investigation and analysis of damage to buildings during the 2003 Bam earthquake Bulletin of the Earthquake Research Institute 79:107-132
O'Reilly GJ, Sullivan TJ (2018) Probabilistic seismic assessment and retrofit considerations for Italian RC frame buildings Bulletin of Earthquake Engineering 16:1447-1485 doi:10.1007/s10518-017-0257-9
Porter K, Farokhnia K, Vamvatsikos D, Cho I (2014) Guidelines for component-based analytical vulnerability assessment of buildings and nonstructural elements. Global Earthquake Model Foundation, Pavia, Italy. doi:10.13117/GEM.VULN-MOD.TR2014.13
Porter K, Kiremidjian A, LeGrue J (2001) Assembly-Based Vulnerability of Buildings and its Use in Performance Evaluation Earthquake Spectra 17:290-312
Ranjbaran F, Hosseini M (2012) Analytical fragility curves of confided masonry buildings. Paper presented at the 15th world conference on earthquake engineering and seismology, 15WCEE secretariat, Lisbon, 24–28 September

Repapis C, Zeris C, Vintzileou E (2006) Evaluation of the seismic performance of existing RC buildings: II. A case study for regular and irregular buildings Journal of Earthquake Engineering 10:429-452 doi:10.1080/13632460609350604
Rota M, Penna A, Strobbia CL (2008) Processing Italian damage data to derive typological fragility curves Soil Dynamics and Earthquake Engineering 28:933-947 doi:https://doi.org/10.1016/j.soildyn.2007.10.010
Sadeghi M, Ghafory-Ashtiany M, Pakdel-Lahiji N (2015) Developing seismic vulnerability curves for typical Iranian buildings Proceedings of the Institution of Mechanical Engineers, Part O: Journal of Risk and Reliability 229:627-640 doi:10.1177/1748006X15596085
Şeşetyan K et al. (2018) The 2014 seismic hazard model of the Middle East: overview and results Bulletin of Earthquake Engineering doi:10.1007/s10518-018-0346-4
Shabakhti N, Biari M (2013) Seismic vulnerability assessment of dual system of steel moment resistant frame and shear wall with fragility curves. Paper presented at the 7th national conference of civil engineering, Zahedan, Iran,
Silva V (2017) Critical Issues on Probabilistic Earthquake Loss Assessment Journal of Earthquake Engineering:1-27 doi:10.1080/13632469.2017.1297264
Silva V, Crowley H, Pagani M, Monelli D, Pinho R (2014a) Development of the OpenQuake engine, the Global Earthquake Model's open-source software for seismic risk assessment Natural Hazards 72:1409-1427 doi:10.1007/s11069-013-0618-x

Silva V, Crowley H, Varum H, Pinho R, Sousa L (2015) Investigation of the characteristics of Portuguese regular moment-frame RC buildings and development of a vulnerability model Bulletin of Earthquake Engineering 13:1455-1490 doi:10.1007/s10518-014-9669-y

Silva V, Crowley H, Varum H, Pinho R, Sousa R (2014b) Evaluation of analytical methodologies used to derive vulnerability functions Earthquake Engineering & Structural Dynamics 43:181-204 doi:doi:10.1002/eqe.2337

Spence R (2007) Earthquake disaster scenario prediction and loss modelling for urban areas. IUSS Press, Pavia. ISBN 978-88-6198-011-2

Tavakoli B, Favakoli A (1993) Estimating the vulnerability and loss functions of residential buildings Natural Hazards 7:155-171 doi:10.1007/bf00680428

Tobita T, Miyajima M, Fallahi A, Alaghebandian R, Ghayamghamian MR (2007) Seismic Intensity Estimation through Questionnaire Survey and Collapse Rates of Various Building Types in the 2003 Bam, Iran, Earthquake Earthquake Spectra 23:841-865 doi:10.1193/1.2790490

Uva G, Porco F, Fiore A (2012) Appraisal of masonry infill walls effect in the seismic response of RC framed buildings: A case study Engineering Structures 34:514-526 doi:https://doi.org/10.1016/j.engstruct.2011.08.043

Vamvatsikos D, Aschheim MA (2016) Performance-based seismic design via yield frequency spectra‡ Earthquake Engineering & Structural Dynamics 45:1759-1778 doi:doi:10.1002/eqe.2727

Villar-Vega M et al. (2017) Development of a Fragility Model for the Residential Building Stock in South America Earthquake Spectra 33:581-604 doi:10.1193/010716eqs005m

Weatherill GA, Silva V, Crowley H, Bazzurro P (2015) Exploring the impact of spatial correlations and uncertainties for portfolio analysis in probabilistic seismic loss estimation Bulletin of Earthquake Engineering 13:957-981 doi:10.1007/s10518-015-9730-5

Xue Q, Wu C-W (2006) Preliminary detailing for displacement-based seismic design of buildings Engineering Structures 28:431-440 doi:https://doi.org/10.1016/j.engstruct.2005.08.015